



Contents lists available at ScienceDirect



# Precambrian Research

journal homepage: [www.elsevier.com/locate/precamres](http://www.elsevier.com/locate/precamres)

## Large variations in lithospheric thickness of western Laurentia: Tectonic inheritance or collisional reworking?

Xuewei Bao\*, David W. Eaton

Department of Geoscience, University of Calgary, Calgary, Alberta T2 N 1N4, Canada

### ARTICLE INFO

#### Article history:

Received 8 October 2014

Received in revised form 9 April 2015

Accepted 3 May 2015

Available online xxx

#### Keywords:

Western Laurentia

Lithospheric evolution

Cratonic keel

Lithosphere–asthenosphere boundary

Surface-wave tomography

### ABSTRACT

The ca. 2.0–1.8 Ga tectonic assembly of Laurentia provides a record of complex processes resulting in amalgamation of distinct lithospheric domains. In global and continental-scale teleseismic tomographic models, however, the subcontinental lithosphere beneath western Laurentia appears to have a deceptively simple structure that lacks a clear correlation with mapped crustal domains. Here we present a new shear-velocity model of the upper mantle beneath western Laurentia through Rayleigh-wave tomography, using data from several newly deployed broadband seismic arrays. Our models show prominent heterogeneities that appear to correlate well with crustal domains and other geophysical observations. The tomographic results delineate high-velocity keel-shaped anomalies beneath the Archean Hearne Province and the Paleoproterozoic Buffalo Head Terrane; these features are inferred to extend to depths of up to 260 km and likely represent ancient thick cratonic roots, whereas relatively thin lithosphere characterizes the adjacent Wabamun domain and Medicine Hat Block. A regional isostatic residual gravity anomaly in the foreland of the Cretaceous–Paleocene southern Canadian Rockies coincides with an area of inferred thick lithosphere in the Hearne Province, suggesting that along-strike variations in flexural rigidity correlate with lithospheric thickness. Taken together, our results suggest that high-amplitude basal topography of the lithosphere–asthenosphere boundary beneath cratons reflects a complex lithospheric evolution that combines effects of both tectonic inheritance and collisional reworking.

© 2015 Elsevier B.V. All rights reserved.

### 1. Introduction

Cratons consist of Precambrian shields and/or contiguous platform regions that are underlain by Precambrian basement rocks (Hoffman, 1988). They form the ancient nuclei of continents, providing a record of planetary evolution spanning billions of years (Griffin et al., 2003), in contrast to oceanic lithosphere with a maximum age of about 200 Myr (Lee et al., 2011). Geophysical and xenolith data demonstrate that cratons are underlain by thick (>160 km), relatively cold mantle keels that are melt-depleted and thus chemically distinct from the convecting mantle (Eaton and Perry, 2013). Compilations of geochronologic data (Carlson et al., 2005; Zhang et al., 2014) also show that formation and collisional assembly of cratons was an episodic process, with distinct global pulses of melt extraction (i.e., formation of juvenile crust) and terrane assembly occurring at 3.2–2.9, 2.7–2.4, 2.0–1.7 and 1.0–0.8 Ga.

In addition to being comprised of a mosaic of distinct lithospheric domains, recent studies also indicate that cratonic lithosphere is layered (Bostock, 1998; Darbyshire et al., 2013; Miller and Eaton, 2010; Yuan and Romanowicz, 2010). It is thus not clear to what extent original formation signatures are preserved throughout the full depth extent of cratonic mantle keels. For example, mid-lithospheric discontinuities imaged using receiver functions beneath several cratonic regions are interpreted to have formed during the imbrication of different lithospheric layers (Bostock, 1998; Miller and Eaton, 2010) with distinctive anisotropic fabrics (Plomerová and Babuška, 2010). Moreover, in the Hudson Bay region near the center of the Laurentian craton in North America, Darbyshire et al. (2013) suggested that the lower half of the mantle keel is characterized by anisotropic fabrics and velocity structure consistent with Proterozoic formation ca. 1.8 Ga, whereas the crust and upper half of the mantle keel are predominantly of Archean age. Furthermore, the destruction of some Archean or Proterozoic cratonic lithospheric mantle, as reported in the North China craton (Menzies et al., 2007; Zhao et al., 2005), is indicative of diverse internal structure of cratons, with spatially varying resistance to convective instabilities. A potentially significant indicator for the stability of a craton is the thickness of its keel, that is, the

\* Corresponding author. Tel.: +1 403 608 7039.

E-mail address: [xubao@ucalgary.ca](mailto:xubao@ucalgary.ca) (X. Bao).

depth to the lithosphere–asthenosphere boundary (LAB), for which estimates using different geophysical methods exhibits significant scatter (Eaton et al., 2009; Fischer et al., 2010; Rychert and Shearer, 2009).

Laurentia, one of the world's largest cratons, was assembled by Paleoproterozoic collision of older blocks cored by Archean lithosphere (Hoffman, 1988). In western Laurentia, the crystalline basement is covered by thick (up to 5.5 km) Phanerozoic sediments. Potential-field, geochronological and seismic reflection/refraction data have elucidated the complex tectonic framework beneath the Western Canada Sedimentary Basin (Ross et al., 1991), the sediment-buried part of Laurentia. However, in global and continental teleseismic tomographic models, the subcontinental lithosphere beneath this region is typically imaged as a high-velocity lid of nearly uniform thickness, exhibiting little apparent correlation with overlying crustal domains (Bedle and van der Lee, 2009; Mercier et al., 2009; Pasquano et al., 2014; Schaeffer and Lebedev, 2014; Yuan et al., 2011). In contrast, a regional teleseismic P-wave tomographic transect imaged a deep-seated high-velocity lithospheric root beneath the southwestern Hearne Province to depths of ~300 km, with relatively low-velocity structure to the north and south (Shragge et al., 2002). The complexity of lithospheric evolution in this region is also evidenced by magnetotelluric observations, which reveal a high-conductivity anomaly beneath the Hearne Province (Ross et al., 2000), in contrast to the typical resistive cratonic structure.

Here we use teleseismic fundamental-mode Rayleigh-wave tomography to construct a new 3D model of the lithospheric shear-wave velocity structure for the study region. We utilize broadband stations from the Canadian National Seismograph Network (CNSN), the Alberta Telemetered Seismograph Network (ATSN), the Canadian Rockies and Alberta Network (CRANE) (Gu et al., 2011), and USArray. Due to the recently augmented station coverage and the ability of surface waves to resolve lithospheric structure, our model has higher resolution in the uppermost mantle compared to previous studies, thus providing new insights into the subcontinental lithospheric architecture and evolution beneath SW Laurentia.

## 2. Tectonic setting

The tectonic evolution of SW Canada records the assembly of the southwestern Laurentian supercontinent in the east and the later accretion of the Cordilleran orogeny to the west (Cook, 1995; Hoffman, 1988). Diverse lithospheric domains beneath our study area in western Canada (Fig. 1) include Archean cratons, Paleoproterozoic terranes and continental margin magmatic arcs that collectively underlie and form the basement of the Western Canada Sedimentary Basin (Ross et al., 1991, 2000). The Great Slave Lake shear zone (GSLsz) in the north, the Snowbird Tectonic Zone (STZ) in the center and the Vulcan Structure (VS) in the south (Eaton et al., 1999) provide a first-order framework for regional subdivision of the crystalline basement. As elaborated below, the lithospheric evolution and inferred relationships between Precambrian domains exhibits strong similarities to active plate margins within a modern plate-tectonic context.

The northwestern part of our study region comprises the Paleoproterozoic Wopmay orogen, which is truncated to the south by the GSLsz, a northeast-trending strike-slip fault that accommodated right-lateral slip of ~700 km during the Proterozoic (Eaton et al., 2004; Hammer et al., 1992; Ross, 2002). From west to east, the Wopmay orogen includes the Nahanni terrane, the Fort Simpson terrane, the Hottah terrane, and the Great Bear magmatic arc (Hildebrand et al., 1987; Villeneuve et al., 1991). The Hottah terrane is composed of magmatic arc and associated sedimentary rocks that formed ca. 1.92–1.90 Ga and collided with the Slave craton

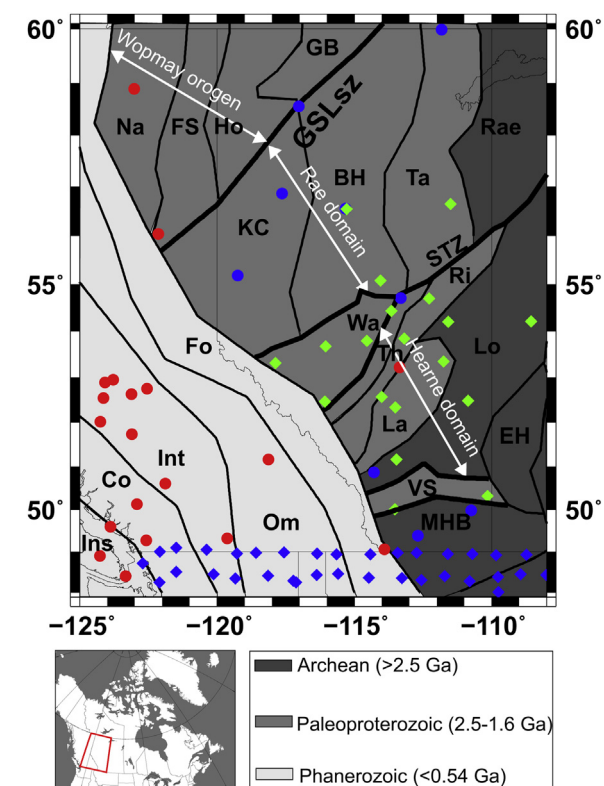


**Fig. 1.** Tectonic map of the study region showing main crustal domains with broadband seismic stations superimposed. Blue circles are Alberta Telemetered Seismic Network, green diamonds are stations from CRANE array, red circles show Canadian National Seismograph Network, and blue diamonds show stations from USArray. Black lines show the boundaries of geological units. Ins – Insular belt; Co – Coast belt; Int – Intermontane belt; Om – Omineca belt; Fo – Foreland fold – thrust belt; Na – Nahanni; FS – Fort Simpson; Ho – Hottah; GB – Great Bear; KC – Ksituan and Chincaga; BH – Buffalo Head terrane; Ta – Taltson; Wa – Wabamun; Th – Thorsby; Ri – Rimbey; La – Lacombe; Lo – Loverna Block; VS – Vulcan Structure; EH – Eyehill High; MHB – Medicine Hat Block; STZ – Snowbird Tectonic Zone; GSLsz – Great Slave Lake shear zone.

ca. 1.90–1.88 Ga. The Great Bear magmatic arc is interpreted to have formed atop the Hottah terrane by east-dipping subduction between 1.88 and 1.84 Ga (Hildebrand et al., 1987). The Fort Simpson terrane is interpreted to represent a ca. 1.85 Ga continental arc produced by westward subduction beneath the Nahanni terrane as it converged with the Hottah terrane before 1.71 Ga (Villeneuve et al., 1991). Based on analysis of drill samples, Villeneuve et al. (1991) suggested that the crust beneath the Fort Simpson terrane may have formed as early as 2.45 Ga.

The Buffalo Head terrane (BHT) is bounded by the STZ to the south and by the GSLsz to the north, and is separated from the Rae craton by the Taltson orogen to the east. Based on Archean inheritance age, Ross (2002) suggested that the BHT is built upon Archean lithosphere, noting that similar basement ages and Nd isotopic signatures for the BHT and the Rae craton indicate that they formed as a single crustal domain by 2.4 Ga. Rifting is evidenced by 2.34 Ga mafic to ultramafic rocks between the BHT and the Rae craton, whereas final accretion of the BHT with the Rae craton is interpreted to have been accommodated by ca. 1.9 Ga eastward subduction, generating the Taltson magmatic zone (Ross, 2002). According to this model, coeval westward subduction to the west of the BHT produced the Ksituan magmatic zone (Fig. 1).

The STZ forms the northwestern boundary of a collage of blocks that accreted to the Archean Hearne Province to form the Hearne domain. The Thorsby domain is interpreted as a remnant ocean basin between the Wabamun domain and the Hearne Province (Ross et al., 2000). Convergence between the Wabamun and Hearne

domains is interpreted to have occurred by southeastward subduction of this ocean basin, generating the ca. 1.85 Ga Rimbey magmatic arc. The Lacombe domain (slightly younger than 2.3 Ga) lies between the Rimbey domain and the Hearne Province and its origin is unclear, with arc marginal or intra-arc basin and foreland-foredeep systems representing two possibilities (Ross et al., 2000). To the east, the Archean Hearne Province is bounded by the ca. 1.8 Ga Trans-Hudson orogen; to the south, it is bounded by the VS, which is interpreted as a Proterozoic collisional suture (Eaton et al., 1999).

Following assembly of those diverse domains, a thick (up to 20 km), ca. 1.1–0.7 Ga Proterozoic passive-margin sequence developed on the western flank of our study area, along the western margin of Laurentia. This margin was further modified by tectonic accretion and orogenic activity in the Canadian Cordillera since the Jurassic (e.g. Cook, 1995). The Phanerozoic evolution of this part of our study region is the subject of a recent study using the same tomographic dataset considered here (Bao et al., 2014).

### 3. Data and methods

#### 3.1. Inter-station phase-velocity measurements from teleseismic Rayleigh waves

Fundamental-mode Rayleigh wave data utilized in this study are from 19 stations of the Canadian National Seismograph Network (CNSN), 9 stations of the Alberta Telemetered Seismograph Network (ATSN), 19 stations of the Canadian Rockies and Alberta Network (CRANE), and 39 stations from USArray (Fig. 1). We selected shallow and intermediate-focus events (depths < 100 km) in a distance range of 20–120° with magnitude larger than 6 during the time period from 2006 to 2013. For each station pair, only earthquakes located within ±5° of the inter-station great circle path were used, in accordance with geometric criteria for the two-station method used to calculate surface-wave dispersion.

The original data were decimated to a sampling rate of 1 Hz and then corrected for the instrument response. Next, we applied frequency-time analysis (Levshin and Ritzwoller, 2001) to the selected seismograms to verify the quality of the group-velocity spectrum and to identify the most reliable period range with robust dispersion measurements. Finally, we measured inter-station phase velocity dispersion using a cross-correlation method (Bao et al., 2011, 2014; Yao et al., 2005, 2006). The robustness of measurements can be influenced by effects such as off-great-circle propagation and scattering (Yoshizawa and Kennett, 2002). In this study, we reduced these potential sources of error by averaging the dispersion curves from multiple source regions for the same station pair. Only dispersion data averaged from at least 3 different events and with standard deviation lower than 2.5% were used for the tomographic inversion.

#### 3.2. Phase-velocity tomography

From the selected path averaged dispersion data, we used a linearized 2D inversion method (Bao et al., 2013; Xu et al., 2013) to construct phase-velocity maps at 1° × 1° grid spacing for the study region. Using ray theory, for each inter-station path, the predicted frequency-dependent travel time  $t(\omega)$  was obtained from the measured phase-velocity distribution  $c(\theta, \phi, \omega)$

$$t(\omega) = \int c^{-1}(\theta, \phi, \omega) ds, \quad (1)$$

where  $\omega$  is frequency and  $\theta, \phi$  specify coordinates of the geographical points along the path. The inversion problem can be expressed in the form of  $\mathbf{Gm} = \mathbf{d} + \mathbf{e}$ , where the vector  $\mathbf{d}$  contains the observed

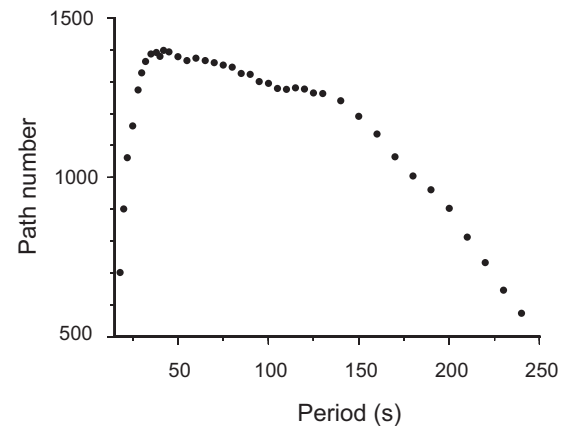


**Fig. 2.** Number of inter-station phase velocity measurements used for tomographic inversion, as a function of period. Most of the measurements are in the period band of 40–150 s, which is primarily sensitive to upper-mantle depths.

travel-time residuals relative to the reference model (usually the average phase velocity at each period) and the vector  $\mathbf{m}$  denotes the model parameters (phase velocity distribution). The sensitivity matrix  $\mathbf{G}$  is known from the forward problem. To estimate  $\mathbf{m}$  we minimized the following objective function

$$E = ||\mathbf{Gm} - \mathbf{d}||^2 + \lambda^2 ||\mathbf{m}||^2 + \varphi^2 ||\mathbf{Lm}||^2. \quad (2)$$

The first term in Eq. (2) measures the data misfit; the second is a model regularization term; and the third term is a Laplacian smoothing constraint, where  $L$  is the 2D finite-difference Laplacian operator, and  $\lambda$  and  $\varphi$  are the damping and smoothing factors, respectively. User-defined regularization parameters were selected based on a series of tests. The parameter  $\lambda$  constrains the inversion in order to reduce deviation from the a priori velocity model, such that a large value of  $\lambda$  results in small perturbations. Similarly, a larger  $\varphi$  results in a smoother model. We selected values for  $\lambda$  and  $\varphi$  that, in our experience, appropriately balance the data misfit, model damping, and smoothness. The resulting sparse system of equations was solved using the LSQR algorithm (Paige and Saunders, 1982).

To evaluate the resolution achieved by our data set in relation to the path coverage, a checkerboard test was performed. The input model consists of  $3^\circ \times 3^\circ$  alternating positive and negative anomalies with magnitude of 5% above or below the average phase velocity at the corresponding period, respectively. Synthetic phase-velocity data were calculated according to the observed inter-station paths, and 2.5% random error in phase velocity was added to each measurement to mimic the errors in real data. These data were then used as input to the same inversion procedure described above, including use of the same damping and smoothing parameters.

The path density used in our tomography at each period is shown in Fig. 2 and the associated path distributions and resolution tests at periods of 50 s, 100 s are plotted in Fig. 3. The number of paths in the period range 22–180 s is >1000, decreasing to >500 at shorter and longer periods, respectively. Fig. 3 shows that the input velocity pattern is generally well recovered by the checkerboard resolution test, except in the northwestern part of our study region. Strong regional variations of path-averaged phase velocities are evident and exhibit coherent patterns at most periods, as illustrated in Fig. 3. In particular, the paths located in the cratonic region are characterized by pronounced high velocities, whereas the paths located in the Cordillera show conspicuous low velocities (Bao et al., 2014). Fig. S1 shows that our dataset is able to resolve an isolated high-velocity anomaly beneath the Hearne domain without significant smearing due to the path distribution.

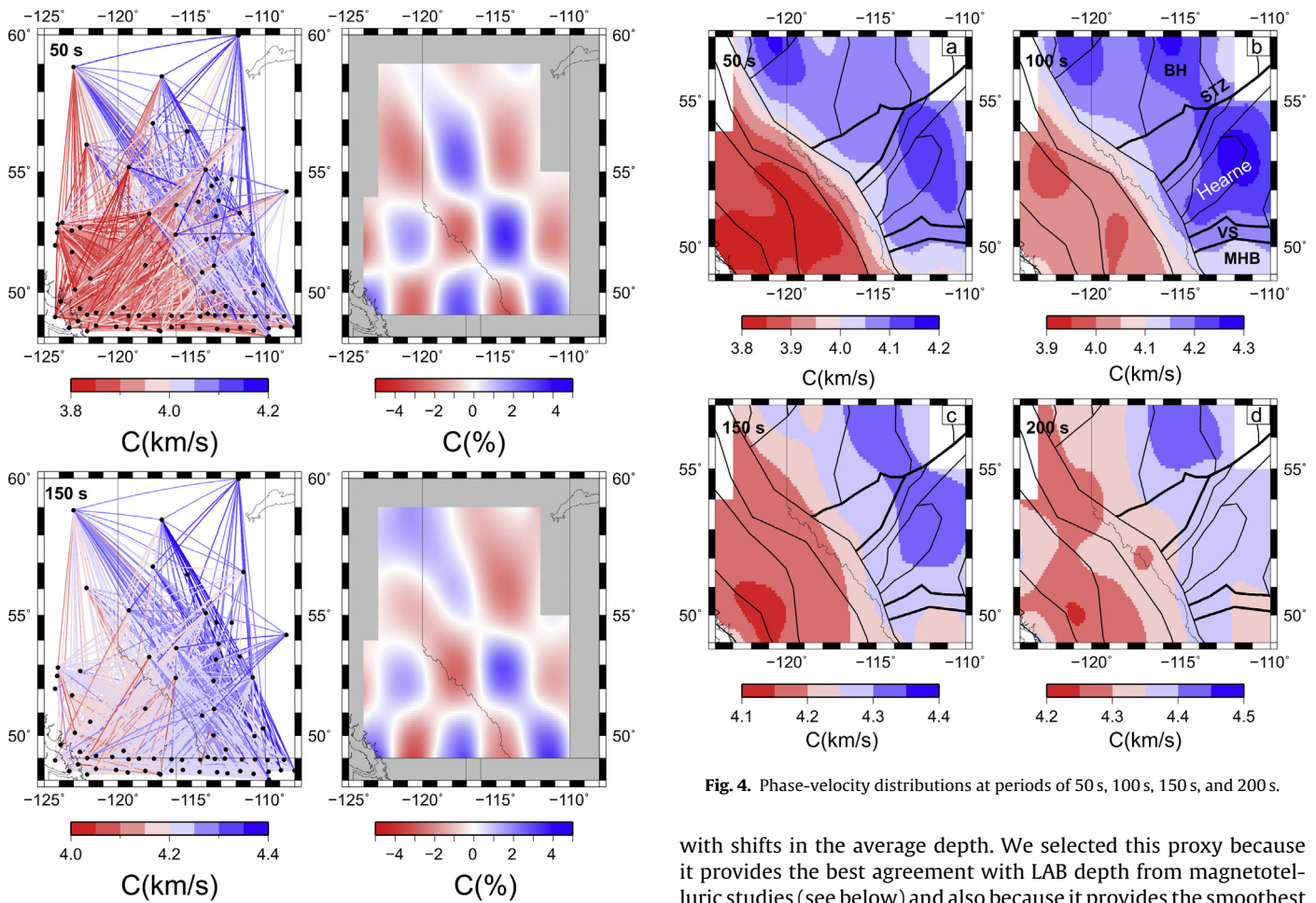


**Fig. 3.** The distribution of inter-station paths (the left panels) and the corresponding checkerboard test results (the right panels) at periods of 50 s (the top panels) and 150 s (the bottom panels). Color scales indicate phase velocity ( $C$ ) variations.

### 3.3. Construction of 3D shear wave velocity model

We inverted shear-wave phase velocities at each grid node to construct a 3D model. The inversion procedure is a first-order approximate linearized inversion-method using a differential inversion scheme (Herrmann and Ammon, 2002), which minimizes the velocity difference between adjacent layers along whilst optimizing the fit between the calculated and observed dispersion data. The initial model for the inversion is modified from AK135 (Kennett et al., 1995) by incorporating the local crustal structure from the Crust 1.0 model (Laske et al., 2013) to refine the velocity structure around the Moho. Figs. S1 and S2 in the supplementary material show two representative 1D shear-velocity models and the related data fit for the Hearne domain and the MHB, respectively.

Although the lithosphere–asthenosphere boundary is a first-order structural discontinuity defining the base of the plate, its definitive identification is often unclear, especially for surface-wave tomographic models from cratonic regions where the velocity structure is usually smoothed. There are two common proxies for LAB based on surface-wave inversion (Eaton et al., 2009): (1) the depth of the strongest negative velocity gradient beneath the high-velocity lid; and (2) a selected contour of positive velocity anomaly (usually 1–2%) above a specified global reference model. Here, we estimate the apparent thickness of the lithosphere based on the depth at which the shear velocity of our model exceeds the shear velocity for model AK135 by 1%. Other proxies for the LAB yield similar spatial patterns of variation in lithospheric thickness, albeit

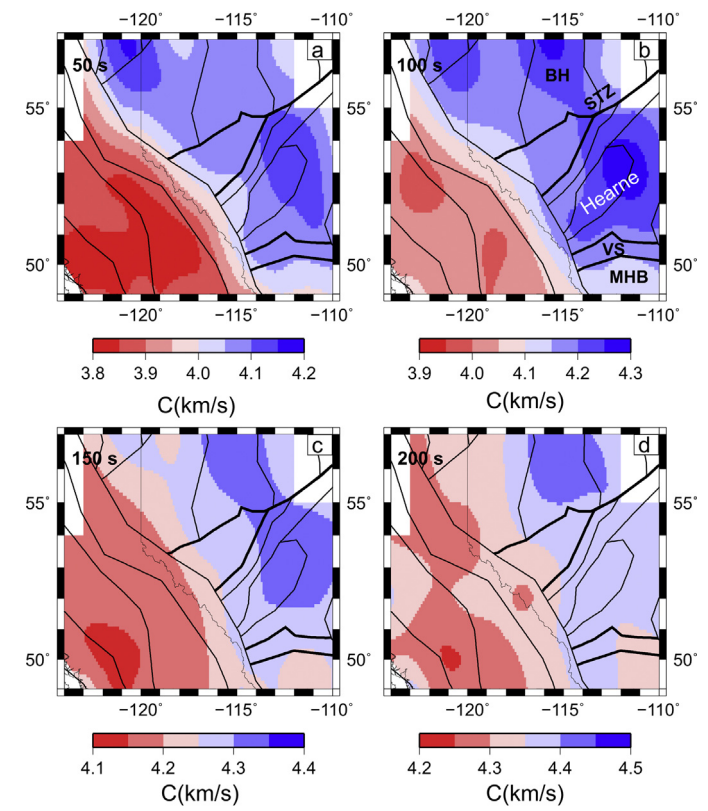


**Fig. 4.** Phase-velocity distributions at periods of 50 s, 100 s, 150 s, and 200 s.

with shifts in the average depth. We selected this proxy because it provides the best agreement with LAB depth from magnetotelluric studies (see below) and also because it provides the smoothest (i.e. least erratic) LAB maps in comparison with the other proxies considered.

## 4. Results

We constructed Rayleigh-wave phase velocity maps at 40 periods from 18 to 240 s. The phase-velocity distribution maps at several representative periods (Fig. 4) illustrate apparent structural variations in the study region. A first-order feature of these maps is a conspicuous change in mantle velocity, going from high velocities within the craton, in the northeast, to much lower velocities beneath the Cordillera in the southwest. The craton edge is remarkably abrupt and is interpreted to be associated with a delamination event at 55 My (Bao et al., 2014); here, our focus is to interpret structural patterns in the interior of the craton. In general, the highest phase velocities occur within both the BHT and the Hearne domain. The VS appears to form a boundary separating the high-velocity Hearne domain from the low-velocity MHB. The STZ is also interpreted as a discernible tectonic boundary that delineates a deep structural contrast between the high-velocity BHT and Hearne domain, as shown in Fig. 4b.

Several representative depth slices and cross sections of our 3D shear velocity model are presented in Figs. 5 and 6. In the uppermost mantle (55 km depth), the principal velocity features are represented by high wavespeed anomalies beneath the Hearne domain and the relatively low wavespeed anomalies in the BHT (Fig. 5a). Starting at a depth of 105 km and continuing deeper, the BHT appears as a relatively high-velocity structure and the MHB begins to manifest as a region of relatively low velocity. At greater depths (155 km and 205 km), the structural heterogeneities of western Laurentia remain conspicuous and correlate well with

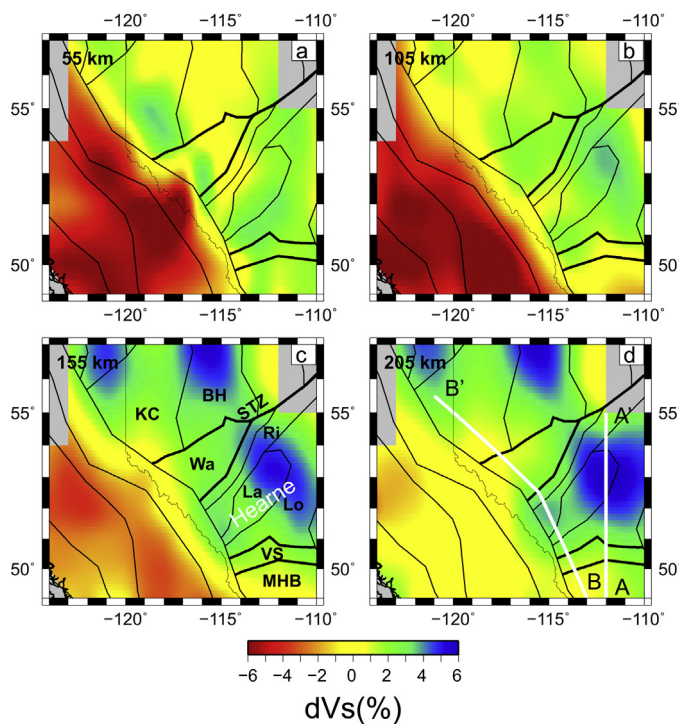


**Fig. 5.** Relative shear velocity compared to the global reference model AK135 (Kennett et al., 1995) at depths of 55 km, 105 km, 155 km, and 205 km.

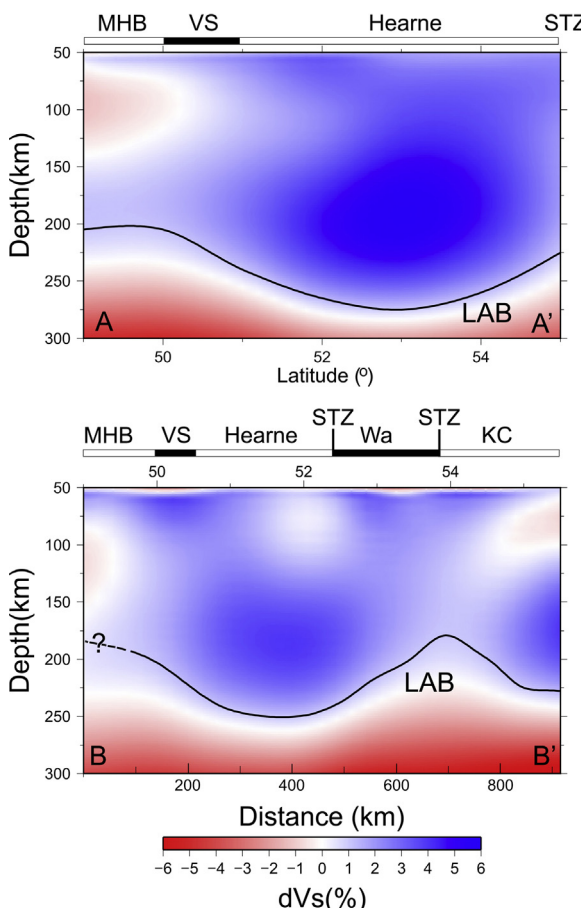


**Fig. 6.** Relative shear-velocity profiles for two cross sections shown in Fig. 5d. The main geological domains are labeled on top of each profile using the same abbreviations in Fig. 1. The black lines represent the estimated lithosphere–asthenosphere boundary (LAB).

the surface geology. In particular, there are two pronounced high-velocity features at this depth range, corresponding to the BHT and the Hearne domain, respectively (Fig. 5). The relative low-velocity structures at these depths mainly occur beneath the MHB and the Wabamun, Ksituan and Chinchaga domains, consistent with a previous P-wave tomographic model (Shragge et al., 2002). These structural features are evident on the velocity profiles (AA', BB' in Fig. 6). The cratonic keels beneath the BHT and the Hearne domain appear (based on our LAB proxy of 1% above AK135) to extend to depths of up to 260 km. Each of these keels appears to be surrounded by relatively low-velocity structures. As shown on profiles AA' and BB', relatively low-velocity features associated with VS and STZ appear to delineate the southern and northern boundaries, respectively, of the high-velocity keel beneath the Hearne domain.

## 5. Discussion

### 5.1. Comparison with other datasets

The shear velocity of the upper lithospheric mantle of the Hearne domain is relatively low compared to typical cratonic mantle lithosphere (Darbyshire et al., 2013; Yuan and Romanowicz, 2010; Yuan et al., 2011; see Fig. S2 in the Supplementary material). Previous magnetotelluric surveys in this region also record anomalous characteristics, revealing layers with unusually high electrical conductivity that have been interpreted to represent the effects of large-scale mantle metasomatism beneath the Hearne domain (Boerner et al., 1999; Nieuwenhuis et al., 2014). Large-scale metasomatism could also explain the relatively low observed shear wavespeeds in the shallow part of the lithospheric mantle beneath the Hearne domain (James et al., 2001).

Similarly, our model indicates that the shear-velocity structure of the lithospheric mantle beneath the MHB is close to continental average model AK135 (Fig. S3), in marked contrast to most Archean cratons, which are characterized by high-velocity mantle lithosphere (e.g., Eaton et al., 2009). This structural feature suggests the absence of typical Archean lithospheric root in this region, as previously inferred by Gorman et al. (2002). Based on the analysis of seismic reflection and refraction data sets, the imaged high-velocity lower crust beneath the MHB (also visible in Fig. S3) has been interpreted as a regional-scale Proterozoic magmatic underplate that thickened the crust. Magmatic underplating of the crust at such a large scale suggests prior (or coeval) removal or modification of the Archean root (Gorman et al., 2002).

The estimated lithospheric thickness beneath SW Laurentia (Fig. 7a) shows considerable variations compared with previous continental-scale tomographic results (Schaeffer and Lebedev, 2014; Yuan et al., 2011). In particular, the lithosphere is thicker beneath the Hearne domain and the BHT, where the LAB extends to >250 km depth, generally consistent with the results of Schaeffer and Lebedev (2014) and Yuan et al. (2011). However, relatively thin lithosphere is apparent in the domains to the east of the northern Rockies (such as the Wabamun domain, the Ksituan and Chincaga domains), where the LAB shallows to ~180 km depth. This area of relative thin lithosphere is not imaged by recent global waveform inversions (Schaeffer and Lebedev, 2014; Yuan et al., 2011), but the shallowing of the LAB south of the VS is apparent in previous waveform inversions using different methods (Schaeffer and Lebedev, 2014; Yuan et al., 2011).

Previous teleseismic P-wave tomography imaged a thick sub-continental root beneath the Hearne domain, with relatively thin lithosphere to the north beneath the Wabamun domain and to the south beneath the MHB (Shragge et al., 2002). These trends of lithosphere thickness anomalies are generally consistent with the strikes of different crustal domains, which change from

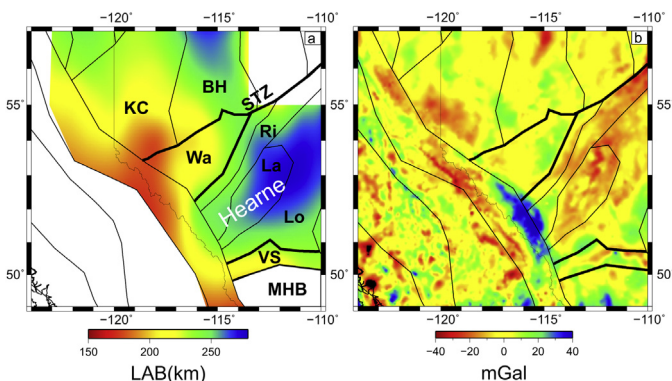


**Fig. 7.** (a) Map view of apparent lithospheric thickness of western Laurentia, estimated from the shear velocity contour in our model that is 1.0% higher than AK135. (b) Residual gravity anomaly map showing a large positive anomaly (blue region) in the Rocky Mountain foreland. This anomaly correlates approximately with relatively thick lithosphere beneath the Hearne domain. Compared with the Cordilleran in the southwest part of the map, gravity anomalies within the craton originate from deeper levels of the crust (e.g. Hope and Eaton, 2002) and thus appear to smoother. Gravity data are provided by Natural Resources Canada and were downloaded from <http://www.nrcan.gc.ca>.

north-south trending in the BHT, to a northeast-southwest orientation in the Hearne domain and to east-west in the MHB (Fig. 7). Lateral variations of lithospheric thickness are also evident on our shear-velocity profiles (Fig. 6), which show large apparent relief of ~70 km in the depth of the LAB over short distance (~100 km) across the STZ and the VS (profiles AA' and BB'). It is interesting to note that further to the east the STZ manifests as a boundary of crustal structure and mantle anisotropy rather than a boundary of mantle wavespeed (Bastow et al., 2014; Thompson et al., 2010), suggesting that different segments of the STZ are characterized by different lithospheric structure.

Although the LAB has been proposed to be a first-order boundary in plate tectonics representing the bottom of the rigid plate, there may be significant discrepancies in depth estimates of LAB from different methods (Eaton et al., 2009). Thus it is necessary to integrate multidisciplinary studies to validate the robustness of the depth estimates of LAB. In our study region, the Hearne domain is imaged as a high-velocity structure extending down to ~260 km depth, which likely represents the bottom of the cratonic lithosphere. Recent 3D magnetotelluric inversion studies reveal that high-conductivity asthenosphere underlying this region occurs below ~250 km (Nieuwenhuis et al., 2014), which agrees well with our results. In addition, the high-velocity structure revealed beneath the BHT indicates that the LAB may extend down to 260 km depth, roughly coincident with the results of a recent magnetotelluric survey in northern Alberta, which indicate that the LAB beneath the BHT occurs at depths of approximately 200–250 km (Türkoğlu et al., 2009). However, based on analysis of garnet lherzolite samples, the LAB of the BHT was estimated to be at 180 km depth in one area of the BHT (Aulbach et al., 2004), shallower than our results and inferences based on magnetotelluric data (Türkoğlu et al., 2009). This apparent discrepancy may indicate that the boundary constrained by xenoliths and xenocrysts represents the base of the depleted part of the cratonic lithosphere (Yuan and Romanowicz, 2010), below which the geophysically imaged cratonic lithosphere extends to greater depth within a basal transition layer.

The inferred variation of lithospheric thickness along the Canadian Rockies foreland exhibits a strong spatial correlation with a large isostatic gravity anomaly (Fig. 7b). This anomaly, which strikes parallel to the Cordilleran front, is derived from a model that incorporates surface topography and geological information on a large regional scale, including crustal thickness and density, (Miles et al., 2001). The anomaly outlines a region that deviates

from isostatic equilibrium based on the Airy–Heiskanen model (Miles et al., 2001). In continental regions, positive isostatic gravity anomalies show features that are not isostatically compensated by crustal thickness variations, thus representing density or buoyancy loads that are supported by lithospheric strength (Burov and Diament, 1995; Zuber et al., 1989). The effective elastic thickness of the lithosphere, which is used to characterize the strength (flexural rigidity) of the lithosphere, shows some positive correlation with the seismically inferred lithospheric thickness, such as in Australia (Fishwick and Reading, 2008; Zuber et al., 1989). The high positive isostatic gravity anomaly in the foreland here closely correlates with the Hearne domain, which has the thickest lithosphere in the region. This correlation suggests that relatively greater lithospheric strength here, manifested as thicker lithosphere, may contribute locally to increased flexural rigidity and isostatic support of the topographic load of the Rocky Mountain foreland region (Burov and Diament, 1995; Zuber et al., 1989). Thus, it appears that during emplacement of thrust sheets during the Cretaceous–Paleocene, flexural response of the lithosphere reflected pre-existing rigidity variations along the strike of the Rocky Mountain foreland consistent with our lithospheric thickness map, providing independent support for our model.

Similar conspicuous lateral variations of lithospheric structure also appear in other cratons. For example, lithospheric thickness changes from ~180 km to almost 280 km beneath the Hudson Bay region near the center of the Laurentian craton, with the greatest lithospheric thicknesses within a region that encompasses both Proterozoic and Archean domains (Darbyshire et al., 2013). Darbyshire et al. (2013) observed that lithospheric thickness does not systematically increase as a simple function of age, which is also the case in our study region. For example, the lithosphere beneath the older Archean MHB is inferred to be significantly thinner than beneath some younger domains in our study area, such as the BHT. Lithosphere models in Australia (Fishwick and Reading, 2008; Simons et al., 1999), Fennoscandia (Bruneton et al., 2004) and the Hudson Bay region of the Canadian shield (Darbyshire and Eaton, 2010) produced from surface-wave tomography similarly indicate that there is no clear relationship between the crustal age and the lithospheric thickness, although Proterozoic lithosphere is thinner than that beneath the Archean cratons in the case of southern Africa (Li and Burke, 2006).

## 5.2. Implications for the evolution of cratonic lithosphere

We consider two generalized end-member models that have been proposed for evolution of cratons. The first model emphasizes the role of tectonic inheritance in the lithospheric evolution of cratons. Based on the lithospheric thickness and anisotropic fabrics modeled from P-wave traveltimes residuals, Plomerová and Babuška (2010) postulated that Precambrian European lithosphere formed primarily through accretion of distinct rigid continental blocks whose original anisotropic fabrics are preserved within the present-day lithosphere. This model implies a lack of pervasive deformation of the lower lithosphere during or after accretion. Coherent lithospheric fabrics that formed during the Archean and survived subsequent Proterozoic tectonic events have also been documented in other cratons, such as the Canadian Shield (Bastow et al., 2011; Kay et al., 1999; Snyder et al., 2013) and the Kaapvaal craton of South Africa (Silver et al., 2001).

An alternative view is that present lithospheric architecture primarily reflects processes that operated during collisional assembly, overprinting the internal structure of older blocks (e.g., Ross et al., 2000). For example, the Hearne domain is characterized by regional granulite-grade metamorphism and pervasive partial melting of the crust during the Paleoproterozoic (ca. 1800 Ma; Ross et al., 2000). Seismic-reflection profiles across the Hearne domain

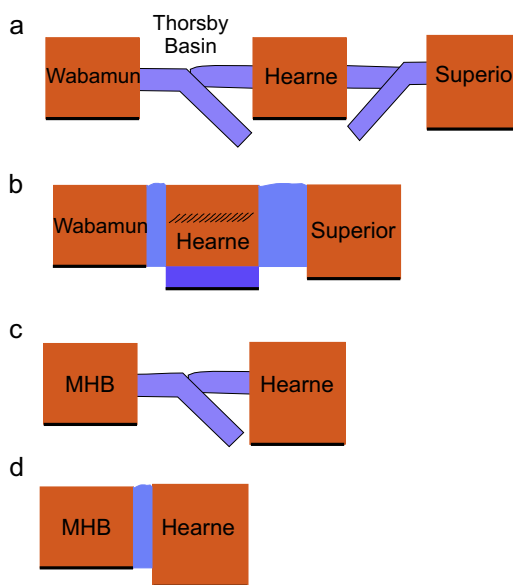


**Fig. 8.** Two models for the Paleoproterozoic cratonic assembly of SW Laurentia. (a) and (b) show tectonic reworking of the Hearne domain with lithospheric basal accretion underneath its original lower lithosphere and the modification of its upper lithospheric mantle; (c) and (d) show preservation of changes in lithospheric thickness by tectonic inheritance during collisional assembly of the Medicine Hat Block (MHB) with the Hearne domain. Thick black line: cratonic lithosphere–asthenosphere boundary (LAB).

reveal a crustal-scale structural fan with reflection fabrics that verge toward the bounding orogens (Ross et al., 1995). Based on these results, Ross et al. (2000) developed a tectonic model involving synchronous inward-dipping subduction zones that formed a ‘tectonic vise’, leading to Proterozoic thickening of the intervening lithosphere.

Collisional thickening processes have been invoked to explain the formation of thick cratonic keels by imbrication of the subducted oceanic lithosphere (Lee et al., 2011). According to this model, subducted oceanic slabs containing a small volume of conductive material (such as hydrogen, carbon) could explain a mid-lithospheric discontinuity characterized by high electrical conductivity beneath the Hearne domain (Nieuwenhuis et al., 2014). Furthermore, an episodic growth model for cratonic lithosphere has also been suggested by other surface wave tomography studies, which show that the lower lithosphere below 160 km depth beneath Laurentia with distinct anisotropic fabrics was formed during or after accretion (Darbyshire et al., 2013; Yuan and Romanowicz, 2010). Mid-lithosphere discontinuities caused by anisotropic or compositional variation have also been imaged by receiver function studies (Bostock, 1998; Miller and Eaton, 2010) providing evidence for slab accretion as a process contributing to the formation of cratonic keels.

Our new tomographic model of southwestern Laurentia suggests that the two end-member models mentioned above may have both contributed to the tectonic evolution of the cratonic keel beneath western Laurentia (Fig. 8). Evidence for preservation of ancient lithospheric fabrics and signatures includes coincidence between crustal and mantle lithospheric boundaries, preservation of distinct trends associated with different lithospheric mantle domains, and changes in lithospheric thickness across inferred sutures such as the VS between the MHB and the Hearne domain. However, there is also evidence from crustal seismic profiles, magnetotelluric studies and relatively low velocities in the shallow lithospheric mantle from our tomographic model suggesting that significant collisional reworking may have occurred in the Hearne domain that contributed to lithospheric thickening. Trapped in a tectonic “vise” formed by two inward-dipping subduction zones

this model suggests that the Hearne domain experienced significant collisional reworking, manifested as pervasive crustal deformation and lithospheric thickening.

In general, while distinct end-member models of tectonic inheritance and collisional reworking may characterize certain areas, our results suggest that preservation of ancient structures and fabrics within older core zones, together with large-scale overprinting during collisional assembly in neighboring domains, may be an archetypal feature of large cratons such as Laurentia.

## 6. Conclusions

This study provides new insights into the structure of the subcontinental lithosphere beneath western Laurentia based on teleseismic Rayleigh-wave tomography results. Our high-resolution tomographic models of shear-wave velocity structure reveal strong heterogeneities in the uppermost mantle beneath SW Laurentia, which agrees well with the known geology and other observations. Apparent lithospheric thickness varies from ~170 km in the Wabamun domain to >230 km beneath the Hearne domain and the Buffalo Head Terrane. Thick lithosphere beneath the Hearne domain closely correlates with a positive isostatic residual gravity anomaly within the foreland of the southern Canadian Rocky Mountains, suggesting that lithospheric thickness may correlate with its flexural rigidity. The boundaries of different crustal domains coincide with different lithospheric mantle domains, elucidating the role of tectonic inheritance in the evolution of cratonic lithosphere. On the other hand, the thick lithosphere beneath the Hearne domain suggests that collisional reworking also acted as an important mechanism in the evolution of the craton, as indicated by previous studies. We conclude that both tectonic inheritance and collisional reworking are key factors in the formation and evolution of the mantle beneath Laurentia.

## Acknowledgements

Seismic data were provided by the Incorporated Research Institutions for Seismology Data Management Center and the Canadian National Data Center. This study was funded by a grant to DWE from the Natural Sciences and Engineering Research Council of Canada (NSERC). Most figures were produced using Generic Mapping Tools (GMT) (Wessel and Smith, 1998). We thank two anonymous reviewers and the Editor Guochun Zhao for their insightful comments. We also appreciate Yu J. Gu and the team of CRANE project for making their seismic data available on the IRIS.

## Appendix A. Supplementary data

Supplementary data associated with this article can be found, in the online version, at <http://dx.doi.org/10.1016/j.precamres.2015.05.010>

## References

- Aulbach, S., Griffin, W.L., O'Reilly, S.Y., McCandless, T.E., 2004. *Genesis and evolution of the lithospheric mantle beneath the Buffalo Head Terrane, Alberta (Canada)*. *Lithos* 77, 413–451.
- Bao, X., Eaton, W.D., Guest, B., 2014. *Plateau uplift in western Canada caused by lithospheric delamination along a craton edge*. *Nat. Geosci.* 7, 830–833.
- Bao, X., Song, X., Xu, M., Wang, L., Sun, X., Mi, N., Yu, D., Li, H., 2013. *Crust and upper mantle structure of the North China Craton and the NE Tibetan Plateau and its tectonic implications*. *Earth Planet. Sci. Lett.* 369/370, 129–137.
- Bao, X., Xu, M., Wang, L., Mi, N., Yu, D., Li, H., 2011. *Lithospheric structure of the Ordos Block and its boundary areas inferred from Rayleigh wave dispersion*. *Tectonophysics* 499, 132–141.
- Bastow, I.D., Thompson, D.A., Wooley, J., Kendall, J.-M., Helffrich, G., Snyder, D.B., Eaton, D.W., Darbyshire, F.A., 2011. *Precambrian plate tectonics: seismic evidence from northern Hudson Bay, Canada*. *Geology* 39, 91–94.
- Bastow, I.D., Eaton, D.W., Kendall, J.M., Helffrich, G., Snyder, D.B., Thompson, D.A., Wooley, J., Darbyshire, F.A., Pawlak, A.E., 2014. *The Hudson Bay Lithospheric*

- Experiment (HuBLE): insights into Precambrian plate tectonics and the development of mantle keels. *Geol. Soc. Lond. Spec. Publ.*, 389, <http://dx.doi.org/10.1144/SP389.7>
- Bedle, H., van der Lee, S., 2009. S velocity variations beneath North America. *J. Geophys. Res.* 114, B07308, <http://dx.doi.org/10.1029/2008JB005949>
- Boerner, D.E., Kurtz, R.D., Craven, J.A., Ross, G.M., Jones, F.W., Davis, W.J., 1999. Electrical conductivity in the precambrian lithosphere of western Canada. *Science* 283 (5402), 668–670, <http://dx.doi.org/10.1126/science.283.5402.668>
- Bostock, M.G., 1998. Mantle stratigraphy and evolution of the Slave province. *J. Geophys. Res.: Solid Earth* 103, 21183–21200.
- Bruneton, M., et al., 2004. Complex lithospheric structure under the central Baltic Shield from surface wave tomography. *J. Geophys. Res.: Solid Earth* 109, B10303, <http://dx.doi.org/10.1029/2003JB002947>
- Brune, J., Dorman, J., 1963. Seismic waves and earth structure in the Canadian Shield. *Bull. Seismol. Soc. Am.* 53, 167–210.
- Burov, E.B., Diament, M., 1995. The effective elastic thickness ( $T_e$ ) of continental lithosphere: what does it really mean? *J. Geophys. Res.: Solid Earth* 100 (B3), 3905–3927, <http://dx.doi.org/10.1029/94JB02770>
- Carlson, R.W., Pearson, D.G., James, D.E., 2005. Physical, chemical, and chronological characteristics of continental mantle. *Rev. Geophys.* 43, RG1001.
- Cook, F.A., 1995. Lithospheric processes and products in the southern Canadian Cordillera: a lithoprobe perspective. *Can. J. Earth Sci.* 32, 1803–1824.
- Darbyshire, F.A., Eaton, D.W., 2010. The lithospheric root beneath Hudson Bay, Canada from Rayleigh wave dispersion: no clear seismological distinction between Archean and Proterozoic mantle. *Lithos* 120, 144–159.
- Darbyshire, F.A., Eaton, D.W., Bastow, I.D., 2013. Seismic imaging of the lithosphere beneath Hudson Bay: episodic growth of the Laurentian mantle keel. *Earth Planet. Sci. Lett.* 373, 179–193.
- Eaton, D.W., Perry, H.K.C., 2013. Ephemeral isopycnicity of cratonic mantle keels. *Nat. Geosci.* 6, 967–970.
- Eaton, D.W., Darbyshire, F., Evans, R.L., Grüter, H., Jones, A.G., Yuan, X., 2009. The elusive lithosphere–asthenosphere boundary (LAB) beneath cratons. *Lithos* 109, 1–22.
- Eaton, D.W., Jones, A.G., Ferguson, I.J., 2004. Lithospheric anisotropy structure inferred from collocated teleseismic and magnetotelluric observations: Great Slave Lake shear zone, northern Canada. *Geophys. Res. Lett.* 31, L19614.
- Eaton, D.W., Ross, G.M., Clowes, R.M., 1999. Seismic-reflection and potential-field studies of the Vulcan structure, western Canada: a paleoproterozoic pyrenees? *J. Geophys. Res.: Solid Earth* 104, 23255–23269.
- Fischer, K.M., Ford, H.A., Abt, D.L., Rychert, C.A., 2010. The lithosphere–asthenosphere boundary. *Ann. Rev. Earth Planet. Sci.* 38, 551–575.
- Fishwick, S., Reading, A.M., 2008. Anomalous lithosphere beneath the Proterozoic of western and central Australia: a record of continental collision and intraplate deformation? *Precambrian Res.* 166, 111–121.
- Gorman, A.R., Clowes, R.M., Ellis, R.M., Henstock, T.J., Spence, G.D., Keller, G.R., Levanter, A., Snelson, C.M., Burianyk, M.J.A., Kanasewich, E.R., Asudeh, I., Hajnal, Z., Miller, K.C., 2002. Deep Probe: imaging the roots of western North America. *Can. J. Earth Sci.* 39 (3), 375–398.
- Griffin, W.L., O'Reilly, S.Y., Abe, N., Aulbach, S., Davies, R.M., Pearson, N.J., Doyle, B.J., Kivi, K., 2003. The origin and evolution of Archean lithospheric mantle. *Precambrian Res.* 127, 19–41.
- Gu, Y.J., Okeler, A., Shen, L., Contenuti, S., 2011. The Canadian Rockies and Alberta Network (CRANE): new constraints on the rockies and western Canada sedimentary basin. *Seismol. Res. Lett.* 82, 575–588.
- Hammer, S., Bowring, S., van Breemen, O., Parrish, R., 1992. Great Slave Lake shear zone, NW Canada: mylonitic record of early proterozoic continental convergence, collision and indentation. *J. Struct. Geol.* 14, 757–773.
- Herrmann, R.B., Ammon, C.J., 2002. Computer Programs in Seismology: Surface Wave, Receiver Functions and Crustal Structure. Saint Louis University, St. Louis, MO, USA.
- Hildebrand, R.S., Hoffman, P.F., Bowring, S.A., 1987. Tectono-magmatic evolution of the 1.9-Ga Great bear magmatic zone, Wopmay orogen, northwestern Canada. *J. Volcanol. Geotherm. Res.* 32, 99–118.
- Hoffman, P.F., 1988. United plates of America, the birth of a craton: early proterozoic assembly and growth of Laurentia. *Ann. Rev. Earth Planet. Sci.* 16, 543–603.
- Hope, J., Eaton, D.W., 2002. Crustal structure beneath the Western Canada sedimentary basin: constraints from gravity and magnetic modelling. *Can. J. Earth Sci.* 39, 291–312.
- James, D.E., Fouch, M.J., VanDecar, J.C., van der Lee, S., Kaapvaal Seismic Group, 2001. Tectospheric structure beneath southern Africa. *Geophys. Res. Lett.* 28, 2485–2488.
- Kay, I., Sol, S., Kendall, J.M., Thomson, C., White, D., Asudeh, I., Roberts, B., Francis, D., 1999. Shear wave splitting observations in the Archean Craton of western Superior. *Geophys. Res. Lett.* 26, 2669–2672.
- Kennett, B.L.N., Engdahl, E.R., Buland, R., 1995. Constraints on seismic velocities in the earth from travel-times. *Geophys. J. Int.* 122, 108–124.
- Laske, G., Masters, G., Ma, Z., Pasynos, M., 2013. Update on CRUST1.0 – A 1-degree global model of earth's crust. *Geophys. Res. Abstracts* 15, Abstract EGU2013-2658.
- Lee, C.T.A., Luffi, P., Chin, E.J., 2011. Building and destroying continental mantle. *Ann. Rev. Earth Planet. Sci.* 39, 59–90.
- Levshin, A.L., Ritzwoller, M.H., 2001. Automated detection, extraction, and measurement of regional surface waves. *Pure Appl. Geophys.* 158, 1531–1545.
- Li, A.B., Burke, K., 2006. Upper mantle structure of southern Africa from Rayleigh wave tomography. *J. Geophys. Res.: Solid Earth* 111, B10303, <http://dx.doi.org/10.1029/2006JB004321>
- Menzies, M., Xu, Y., Zhang, H., Fan, W., 2007. Integration of geology, geophysics and geochemistry: a key to understanding the North China Craton. *Lithos* 96, 1–21.
- Mercier, J.P., Bostock, M.G., Cassidy, J.F., Dueker, K., Gaherty, J.B., Garnero, E.J., Revenaugh, J., Zandt, G., 2009. Body-wave tomography of western Canada. *Tectonophysics* 475, 480–492.
- Miles, W.F., Roest, W.R., Vo, M.P., 2001. Isostatic Residual of Gravity Anomalies, Canada. *GSC Open File 4160*.
- Miller, M.S., Eaton, D.W., 2010. Formation of cratonic mantle keels by arc accretion: evidence from S receiver functions. *Geophys. Res. Lett.* 37, L18305.
- Nieuwenhuis, G., Unsworth, M.J., Pana, D., Craven, J., Bertrand, E., 2014. Three-dimensional resistivity structure of Southern Alberta, Canada: implications for precambrian tectonics. *Geophys. J. Int.* 197, 838–859.
- Paige, C.C., Saunders, M.A., 1982. LSQR: an algorithm for sparse linear equations and sparse least squares. *ACM Trans. Math. Softw.* 8, 43–71.
- Pasyanos, M.E., Masters, T.G., Laske, G., Ma, Z., 2014. LITHO 1.0: an updated crust and lithospheric model of the Earth. *J. Geophys. Res.: Solid Earth* 119, 2153–2173.
- Plomerová, J., Babuška, V., 2010. Long memory of mantle lithosphere fabric – European LAB constrained from seismic anisotropy. *Lithos* 120, 131–143.
- Ross, G.M., 2002. Evolution of Precambrian continental lithosphere in Western Canada: results from Lithoprobe studies in Alberta and beyond. *Can. J. Earth Sci.* 39, 413–437.
- Ross, G.M., Eaton, D.W., Boerner, D.E., Miles, W., 2000. Tectonic entrapment and its role in the evolution of continental lithosphere: an example from the Precambrian of western Canada. *Tectonics* 19, 116–134.
- Ross, G.M., Parrish, R.R., Villeneuve, M.E., Bowring, S.A., 1991. Geophysics and geochronology of the crystalline basement of the Alberta Basin, western Canada. *Can. J. Earth Sci.* 28, 512–522.
- Ross, G.M., Milkereit, B., Eaton, D.W., White, D., Kanasewich, E.R., Burianyk, M.J., 1995. Paleoproterozoic collisional orogen beneath the western Canada sedimentary basin imaged by Lithoprobe crustal seismic-reflection data. *Geology* 23, 195–199.
- Rychert, C.A., Shearer, P.M., 2009. A global view of the lithosphere–asthenosphere boundary. *Science* 324, 495–498.
- Schaeffer, A.J., Lebedev, S., 2014. Imaging the North American continent using waveform inversion of global and USArray data. *Earth Planet. Sci. Lett.* 402, 26–41, <http://dx.doi.org/10.1016/j.epsl.2014.05.014>
- Shragge, J., Bostock, M.G., Bank, C.G., Ellis, R.M., 2002. Integrated teleseismic studies of the southern Alberta upper mantle. *Can. J. Earth Sci.* 39, 399–411.
- Silver, P.G., Gao, S.S., Liu, K.H., 2001. Mantle deformation beneath southern Africa. *Geophys. Res. Lett.* 28, 2493–2496.
- Simons, F.J., Zielhuis, A., van der Hilst, R.D., 1999. The deep structure of the Australian continent from surface wave tomography. In: van der Hilst, R.D., McDonough, W.F. (Eds.), *Developments in Geotectonics*. Elsevier, pp. 17–43.
- Snyder, D.B., Berman, R.G., Kendall, J.M., Sanborn-Barrie, M., 2013. Seismic anisotropy and mantle structure of the Rae craton, central Canada, from joint interpretation of SKS splitting and receiver functions. *Precambrian Res.* 232, 189–208.
- Türkoğlu, E., Unsworth, M., Pana, D., 2009. Deep electrical structure of northern Alberta (Canada): implications for diamond exploration. *Can. J. Earth Sci.* 46, 139–154.
- Thompson, D.A., Bastow, I.D., Helffrich, G., Kendall, J.M., Wookey, J., Snyder, D.B., Eaton, D.W., 2010. Precambrian crustal evolution: seismic constraints from the Canadian Shield. *Earth Planet. Sci. Lett.* 297, 655–666.
- Villeneuve, M.E., Thériault, R.J., Ross, G.M., 1991. U-Pb ages and Sm-Nd signature of two subsurface granites from the Fort Simpson magnetic high, northwest Canada. *Can. J. Earth Sci.* 28, 1003–1008.
- Wessel, P., Smith, W.H.F., 1998. New, improved version of the Generic Mapping Tools Released. *EOS Trans. AGU* 79 (47), 579, <http://dx.doi.org/10.1029/98EO00426>
- Xu, Z.J., Song, X.D., Zheng, S.H., 2013. Shear velocity structure of crust and uppermost mantle in China from surface wave tomography using ambient noise and earthquake data. *Earth Sci.* 26 (5), 267–281.
- Yao, H., Xu, G., Zhu, L., Xiao, X., 2005. Mantle structure from interstation Rayleigh wave dispersion and its tectonic implication in western China and neighboring regions. *Phys. Earth Planet. Inter.* 148, 39–45.
- Yao, H., Van Der Hilst, R.D., De Hoop, M.V., 2006. Surface-wave array tomography in SE Tibet from ambient seismic noise and two-station analysis – I. Phase velocity maps. *Geophys. J. Int.* 166, 732–744.
- Yoshizawa, K., Kennett, B.L.N., 2002. Determination of the influence zone for surface wave paths. *Geophys. J. Int.* 149, 440–453.
- Yuan, H., Romanowicz, B., 2010. Lithospheric layering in the North American craton. *Nature* 466, 1063–1068.
- Yuan, H., Romanowicz, B., Fischer, K.M., Abt, D., 2011. 3-D shear wave radially and azimuthally anisotropic velocity model of the North American upper mantle. *Geophys. J. Int.* 184, 1237–1260.
- Zhang, H.F., Wang, J.L., Zhou, D.W., Yang, Y.H., Zhang, G.W., Santosh, M., Yu, H., Zhang, J., 2014. Hadean to Neorachean episodic crustal growth: detrital zircon records in paleoproterozoic quartzites from the southern North China craton. *Precambrian Res.* 254, 245–257.
- Zhao, G.C., Sun, M., Wilde, S.A., Li, S.Z., 2005. Late archean to paleoproterozoic evolution of the North China craton: key issues revisited. *Precambrian Res.* 136, 177–202.
- Zuber, M.T., Bechtel, T.D., Forsyth, D.W., 1989. Effective elastic thicknesses of the lithosphere and mechanisms of isostatic compensation in Australia. *J. Geophys. Res.* 94, B7.